Transport Properties of GaAs Obtained from Photoemission Measurements*

L. W. JAMES† AND J. L. MOLL
Stanford University, Stanford, California
(Received 20 December 1968)

Using the technique of high-resolution energy-distribution analysis of electrons photoemitted from a cleaved GaAs surface coated with a layer of Cs, we have been able to determine many of the transport properties of GaAs which are important in the operation of the GaAs-Ca-O photocathode and other GaAs devices. A two-minima diffusion model is presented which explains the photon energy dependence of the photocathode yield near threshold. Electron diffusion lengths for the Γ_1 and X_1 minima have been determined from the spectral shape of quantum yield as a function of temperature and carrier concentration for heavily doped p-type material. The hot-electron scattering length for equivalent intervalley scattering has been measured by comparison with a computer scattering model. The coupling constant for equivalent intervalley scattering has been calculated from the hot-electron scattering length. The coupling constant for scattering between the Γ_1 and X_1 minima is calculated from the X_1 diffusion length. These results, along with other recent data, are used to calculate the temperature dependence of the mobility in the X_1 valleys and the intervalley scattering time. The temperature dependence of the energy spacing of the Γ_1 and X_1 valleys has been measured. The escape probability for the photocathode and the shape of the energy distribution curves is explained by a model which includes optical phonon scattering in the band-bending region, reflection at the surface, trapping in surface states, and lifetime broadening.

I. INTRODUCTION

HEAVILY doped p-type GaAs cleaved in an ultrahigh vacuum and coated with cesium has a low enough work function to permit photoexcited electrons from all energies within the conduction band to escape, giving a high quantum yield at all photon energies greater than the band gap and producing a high-efficiency photocathode.[1] The application of additional oxygen-cesium layers increases the efficiency over that obtained with cesium alone.

High-resolution measurement of emitted electron energy distributions provides a valuable tool for studying the details of the photoemission process. In this paper the results obtained using this technique will be discussed, principally in terms of determining electron transport properties.

II. EXPERIMENTAL METHODS

Samples are prepared in an ultrahigh-vacuum cleaving chamber. A single crystal of commercially available boat-grown p^+ GaAs 1 cm square by $1\frac{1}{2}$ cm long is mounted on a moveable rod, aligned such that the (110) face (the cleavage plane) faces a window on the front of the chamber. After pumping the chamber down to a pressure of 10^{-11} Torr, the crystal is moved into position between a tungsten carbide blade and an annealed copper anvil. Pressure is applied between the blade and anvil until the crystal cleaves, giving a mirrorlike surface with a few cleavage lines.

Cesium is applied to the freshly cleaved surface from a cesium chromate channel source while monitoring the photocurrent produced by a dim white light. As cesium is applied, the photocurrent increases approximately exponentially until a peak sensitivity is reached.

For those samples treated with additional oxygen-cesium layers, after applying the first layer of cesium (as described above), oxygen is leaked into the chamber at a partial pressure of 2×10^{-8} Torr for a period of 20 min. During this time the photocurrent decreases. The oxygen supply is then turned off, and the chamber is allowed to pump back to a low pressure. After the photocurrent has stabilized, cesium is again applied until a peak in sensitivity is reached. This process gives an additional "oxygen-cesium layer" and may be repeated as many times as desired to obtain multiple oxygen-cesium layers, referred to as $(O+Cs)^n$ for n additional layers.

After preparation, the sample is moved inside a collector can where measurements are made. Light from a monochromator is focused to a small spot in the center of the cleaved crystal face. A retarding potential is applied between the sample and the approximately spherical collector can, and the current emitted by the sample is measured as the retarding potential is increased. The derivative of sample current with respect to retarding voltage is the energy-distribution curve. The derivative is taken electronically using a small (0.01 V peak-to-peak) ac signal in series with the retarding voltage and a lock-in amplifier.

Figure 1 shows a typical set of experimental energy-distribution curves taken at room temperature for a range of photon energies from 1.4 to 3.0 eV.

III. TWO-MINIMA DIFFUSION MODEL FOR PHOTOEMISSION NEAR THRESHOLD

Figure 2 shows a band diagram for a p^+ GaAs crystal coated with a layer of cesium. The bands are bent

* Work supported by the Advanced Research Projects Agency through the Center for Materials Research at Stanford University, Stanford, Calif., and by the U. S. Army Night Vision Laboratory, Ft. Belvoir, Va.
† Present address: Central Research, Varian Associates, Palo Alto, Calif.
[1] J. J. Scheer and J. Van Laar, Solid State Commun. 3, 189 (1965).

near the surface and the work function is lowered sufficiently that the vacuum level is below the bottom of the conduction band in the bulk of the material. Near threshold the absorption coefficient for light is small enough that only a few percent of the light is absorbed in the band-bending region, and almost all photoexcitation takes place in the bulk of the material. The hot-electron scattering length is also short compared with the optical absorption length, so that photoexcited electrons thermalize in a conduction band minima, then diffuse to the band-bending region, where they are accelerated toward the surface and emitted.

Figure 3 shows a band structure for GaAs near the band gap. Photoexcitation in this material requires conservation of **k** vector and energy, giving vertical transitions between states in the valence bands and states in the conduction bands which differ in energy by $h\nu$, where $h\nu$ is the photon energy. Photoexcited electrons will have a range of final energies which could in principle be determined accurately from a knowledge of the band structure and optical-transition matrix elements throughout the Brillouin zone. Rather than work with the actual final excited energy distribution, we will make approximations at this point.

For low photon energies, such as shown at (a) in Fig. 3, all photoexcitation will be to final states lower in energy than the X_1 minima and thermalization will occur into the Γ_1 minima. For higher photon energies, such as shown at (b), some excitation will be to energies above 1.75 eV and some to energies below 1.75 eV. An electron excited above 1.75 eV will rapidly scatter into X_1 and thermalize there,[2] owing to the higher density of states in X and the value of the coupling coefficient for Γ_1 to X_1 scattering. The fraction which is excited to energies greater than 1.75 eV will be defined as F_X. These electrons are assumed to travel only a very short distance through the crystal before thermalizing in X. The remaining fraction of excited electrons, F_Γ, are assumed to rapidly thermalize in the Γ minima, F_Γ and F_X are shown in Fig. 4.

Above the band gap, F_X and F_Γ were determined by a graphical construction taking into account energy- and **k**-vector-conserving transitions from the highest three valence bands to the lowest conduction band. The graphical construction was done using equal energy contours for these four bands in the (110) and (100) planes obtained from the Herman *et al.* band-structure calculation[3] corrected for spin-orbit splitting,

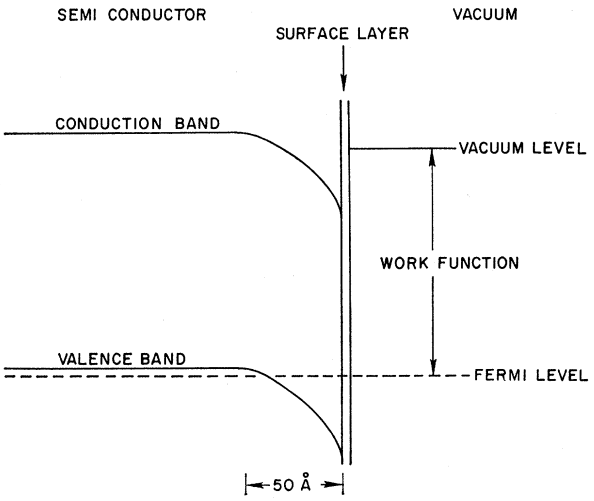

FIG. 2. Band-bending diagram showing the effects of a layer of cesium applied to a p^+ GaAs surface.

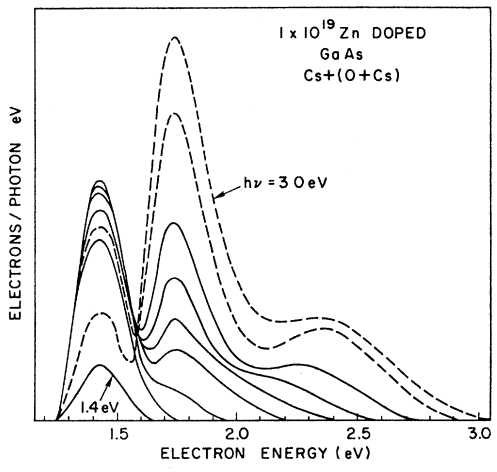

FIG. 1. Normalized and smoothed experimental energy-distribution curves for a 1×10^{19}/cm^3 Zn-doped GaAs crystal with a Cs+(O+Cs) surface treatment shown for increments of 0.2 eV for a photon energy range of 1.4–3.0 eV. The 2.8- and 3.0-eV curves are shown dashed for clarity.

[2] R. C. Eden, J. L. Moll, and W. E. Spicer, Phys. Rev. Letters 18, 597 (1967).

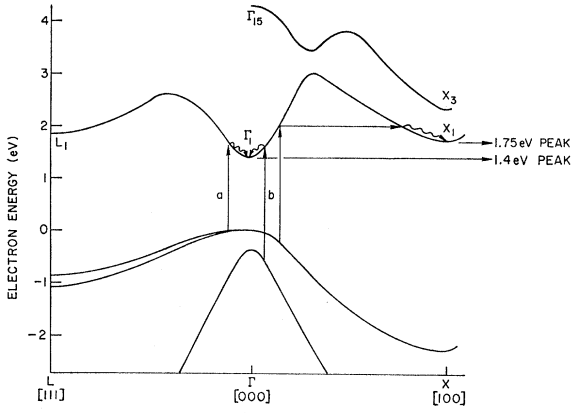

FIG. 3. GaAs band structure near the energy gap showing examples of photoexcitation, scattering, and thermalization in the Γ_1 and X_1 minima. For photon energies below 1.7 eV (a), all electrons thermalize in the Γ_1 minima. Above 1.7 eV (b), some electrons are excited to a high-enough energy to thermalize in X_1.

[3] F. Herman, R. L. Kortum, C. D. Kuglin, J. P. Van Dyke, and S. Skillman, in *Methods of Computational Physics*, edited by B. Alder, S. Fernbach, and M. Rotenberg (Academic Press Inc., New York, 1968), Vol. 8.

X-Γ spacing, and band tailing. Constant matrix elements were assumed for transitions from the highest two valence bands, while the matrix elements for transitions from the third highest valence band were assumed to be a factor of 3 smaller. It should be noted that while the shapes of these curves are qualitatively correct, the actual numbers must be considered approximate due to the assumption of constant matrix elements, the use of only two planes rather than the entire Brillouin zone, the approximate nature of the graphical technique used, and the possible errors in the band-structure calculation. The major effect of changes in these numbers is to change the X diffusion length as calculated later. Below the band gap F_Γ drops below unity as a significant fraction of the photons are absorbed by free carriers (holes) rather than by band-to-band transitions.[4]

Examination of the experimental energy-distribution curves shows that for photon energies from threshold at 1.4 (near-infrared)–2.3 eV (blue-green) almost all emitted electrons are thermalized in either the Γ_1 or X_1 minima, while for higher photon energies a significant number of higher-energy unthermalized electrons may be seen in the distribution. Also, above 2.3 eV, α becomes large enough that excitation in the band-bending region may no longer be neglected. Below 2.3 eV we need to consider only those electrons generated in the bulk crystal, and these are assumed to be thermalized in either the Γ or X minima so we may solve for electron transport in terms of the 1-dimensional coupled diffusion equations for these minima.

$$-D_\Gamma\frac{\partial^2 n_\Gamma}{\partial y^2}+\frac{n_\Gamma}{\tau_{\Gamma V}}=\frac{n_X}{\tau_{X\Gamma}}+I(1-R)F_\Gamma\alpha e^{-\alpha y}, \quad (\Gamma \text{ equation}) \quad (3.1)$$

$$-D_X\frac{\partial^2 n_X}{\partial y^2}+\frac{n_X}{\tau_{X\Gamma}}=I(1-R)F_X\alpha e^{-\alpha y}, \quad (X \text{ equation}) \quad (3.2)$$

where y is the distance into the crystal.

The first term in each equation is the diffusion term, where D is the diffusion coefficient. The second term is the rate at which carriers are lost from each minima. $\tau_{\Gamma V}$ is the recombination time from the Γ minima to the valence band (or to traps). $\tau_{X\Gamma}$ is the relaxation time for scattering from the X_1 minima to the Γ_1 minima. $n_X/\tau_{X\Gamma}$ is a rate of generation term in the Γ equation as well as a rate of loss term in the X equation. The last term is the rate of generation by photoexcitation, where I is the incident light intensity, R is the reflectivity, and α is the optical absorption coefficient. The assumptions implicit in writing these equations are that there is no recombination from X directly to the valence band, and that the distance an electron travels through the crystal while thermalizing is short compared with $(1/\alpha)$ and the diffusion lengths.

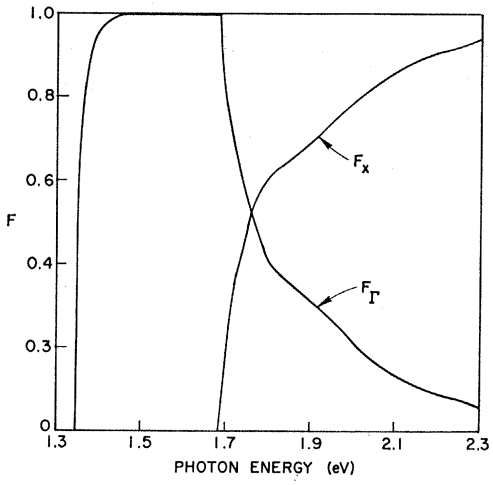

FIG. 4. Fraction of photoexcited electrons which thermalize in each minima, calculated from the GaAs band structure, corrected for the presence of an impurity band.

Using the band-bending region as a boundary condition, we may solve these equations for the current density flowing into the band-bending region, giving

$$J_X=\frac{qI(1-R)F_X}{1+1/\alpha L_X} \quad (3.3)$$

and

$$J_\Gamma=\frac{qI(1-R)}{1+1/\alpha L_\Gamma}\left[F_\Gamma+\frac{F_X L_\Gamma}{\alpha L_X(L_\Gamma+L_X)(1+1/\alpha L_X)}\right], \quad (3.4)$$

where the diffusion lengths are given by

$$L_X=(D_X\tau_{X\Gamma})^{1/2}, \quad (3.5)$$

$$L_\Gamma=(D_\Gamma\tau_{\Gamma V})^{1/2}. \quad (3.6)$$

Of that current flowing into the band-bending region, a certain fraction, given by the escape probability P, will be emitted into the vacuum. P will be a function of both surface treatment and electron energy. The photoelectric quantum efficiency, or yield, is then given for each minima by

$$Y_X=\frac{P_X J_X}{qI(1-R)}=\frac{P_X F_X}{1+1/\alpha L_X}, \quad (3.7)$$

$$Y_\Gamma=\frac{P_\Gamma J_\Gamma}{qI(1-R)}=\frac{P_\Gamma}{1+1/\alpha L_\Gamma}\times\left[F_\Gamma+\frac{F_X L_\Gamma}{\alpha L_X(L_\Gamma+L_X)(1+1/\alpha L_X)}\right]. \quad (3.8)$$

Everything is known in these equations except the diffusion lengths L_X and L_Γ and the escape probabilities

[4] C. M. Chang, Ph.D. thesis, Stanford University, 1964 (unpublished).

P_X and P_Γ. The X and Γ yields may be obtained experimentally from the energy-distribution curves. Examining the yield equations, we see that the magnitude of the yield versus photon energy curves is determined by the escape probability, while the shape of the curves is determined by the diffusion length. Thus P_X and L_X may be determined uniquely from the experimental X-yield curve, and P_Γ and L_Γ may be obtained from the Γ-yield curve. Figure 5 and the solid curve in Fig. 6 indicate the match between theory and experiment for the X and Γ minima, respectively, where the points are room-temperature experimental data for a $1\times10^{19}/\text{cm}^3$ Zn-doped crystal, vacuum cleaved and coated with cesium plus an additional oxygen-cesium layer; and the solid curves are plots of the theoretical yield equations using the parameters $P_\Gamma=0.18$, $L_\Gamma=1.573\ \mu$, $P_X=0.54$, and $L_X=0.03\ \mu$.

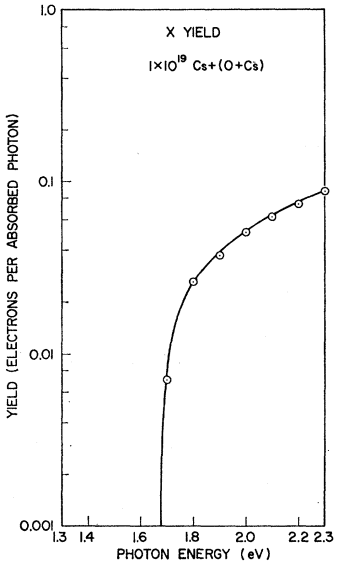

FIG. 5. Theoretical (solid line) and experimental (points) yields from the X_1 minima in a $1\times10^{19}/\text{cm}^3$ Zn-doped GaAs crystal with a Cs+(O+Cs) surface treatment.

For this theory to be physically meaningful, the diffusion length should be a property of the bulk crystal, while the escape probability should be a function of surface treatment. That this is in fact the case is shown in Fig. 7, where the match between theory and experiment is shown for various surface treatments on the same crystal. All theoretical curves use the same diffusion length of 1.573 μ, while the escape probability varies over a range of almost 20. In both Fig. 6 and the lowest curve in Fig. 7, there is a slight discrepancy between theory and experiment. A probable reason for at least part of this discrepancy is the assumption of complete thermalization of Γ electrons in a distance short compared with other relevant distances. Γ electrons which are not completely thermalized before reaching the band-bending region would be expected

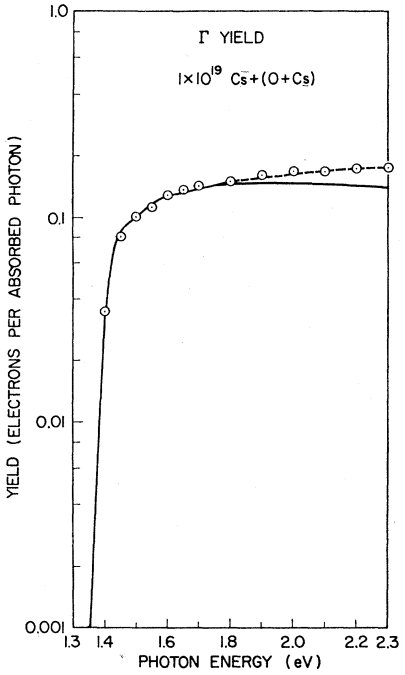

FIG. 6. Experimental yield (points) for the Γ_1 minima in a $1\times10^{19}/\text{cm}^3$ Zn-doped GaAs crystal with a Cs+(O+Cs) surface treatment, compared with Eq. (3.8) (solid curve) and Eq. (3.9) (dashed curve).

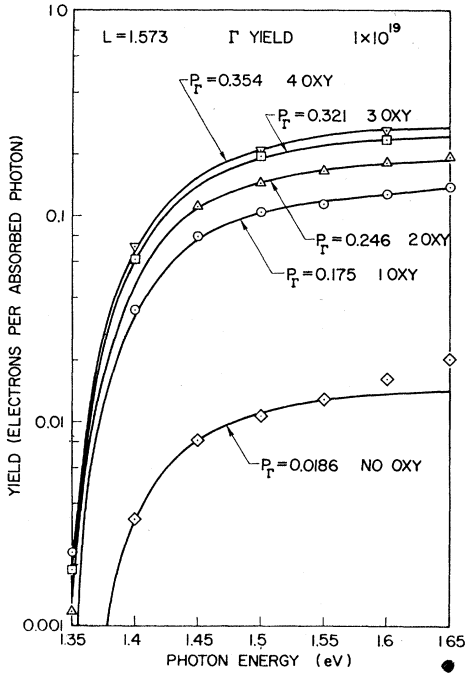

FIG. 7. Comparison between theoretical and experimental Γ_1 yields for various surface treatments, demonstrating that the measured diffusion length is a property of the bulk crystal and is independent of surface treatment.

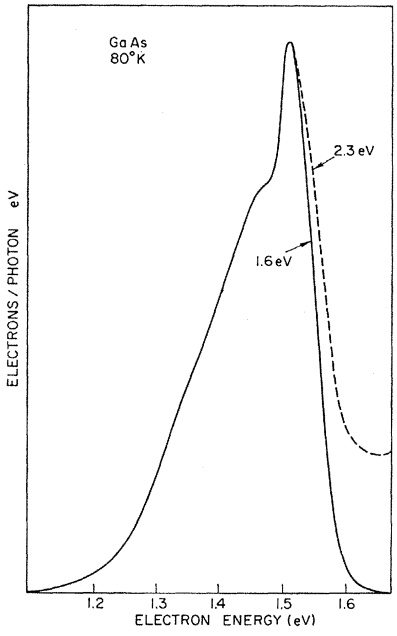

FIG. 8. Comparison of the Γ_1 peak in 80°K energy-distribution curves for photon energies of 1.6 and 2.3 eV, showing evidence for the lack of complete thermalization with 2.3-eV excitation.

to have a higher escape probability than those which are thermalized. As the absorption length decreases (photon energy increased), the departure from thermalization becomes more significant. Figure 8 shows the comparison between energy distributions for photon energies of 1.6 and 2.3 eV at 80°K. The increased number of electrons at the high-energy end of the distribution gives experimental evidence for this departure. The increased escape probability caused by lack of complete thermalization may be taken into account empirically by adding an additional parameter P_Γ', which is slightly larger than P_Γ to the Γ yield equation, giving

$$Y_\Gamma=(1+1/\alpha L_\Gamma)^{-1}[F_\Gamma P_\Gamma+F_X P_\Gamma'/(1+\alpha L_X)] \quad \text{for } L_X \ll L_\Gamma. \tag{3.9}$$

The dashed curve in Fig. 6 is drawn using this equation with $P_\Gamma'=0.22$. (The other parameters are the same as previously listed.) The match between theory and experiment is now quite good.

Using the least-squares fit between this theory and experimental data for several samples, we have obtained the Γ diffusion lengths which are shown in Table I.

TABLE I. Measured Γ diffusion lengths for boat-grown Zn-doped material.

Carrier concentration (cm^{-3})	Diffusion length (μ) 300°K	80°K
1×10^{19}	1.6±0.2	
3×10^{19}	1.2±0.2	1.0±0.3
4×10^{19}	1.0±0.2	

The X diffusion length is found to be independent of doping and is measured to be 0.03 μ at room temperature. As indicated earlier, the measured value of the X diffusion length depends on the function F_X. Without doing an exact calculation knowing the values of the optical-transition matrix elements, it is difficult to estimate the possible errors in F_X. It is possible, however, to calculate the maximum possible error in the value of L_X. The yield in the X minima is given by Eq. (3.7). Solving for L_X, we obtain

$$L_X=Y_X/\alpha(P_X F_X-Y_X). \tag{3.10}$$

At 2.3 eV for this sample, $Y_X=0.087$ and $\alpha=0.7032\times10^5$/cm. By estimating the maximum and minimum limits of $P_X F_X$, we may estimate the possible range of L_X. 2.3 eV was chosen because at 2.3 eV all transitions from the top two valence bands are included in F_X, and all transitions from the third highest valence band are included in F_Γ, independent of small errors in the band-structure calculation.

The maximum possible value of F_X is 1.0. Pseudopotential calculations[5] indicate that the matrix elements for transitions from the third highest valence band are smaller than for transitions from the top two valence bands by about a factor of 3. If this ratio is off by a factor of 2, that is if a ratio of 1.5 is the correct ratio, then F_X (2.3 eV)=0.82, giving a lower limit for F_X.

The maximum yield for this sample and surface treatment is about 0.5 (for photon energies low enough that carrier multiplication is not possible). The Γ yield in this range (around 3.0 eV) is at a minimum value of 0.06 electrons/(absorbed photon). The "average" escape probability for X and high-energy electrons is then 0.6. Assuming that escape probability is a monotonically increasing function of energy, we have 0.6 for the maximum value of P_X.

For an optimum surface treatment of cesium plus six additional oxygen-cesium layers on this sample $P_\Gamma=0.360$, and the vacuum level is less than 0.3 eV below the Γ_1 minima. Again assuming a monotonically increasing escape function, $P_X>0.360$. If we take into account absorption in the six oxygen-cesium layers, and the fact that escape probability does increase with energy, a minimum value of 0.45 for P_X is still a conservative lower limit. From these considerations

$$0.024\,\mu<L_X<0.044\,\mu, \tag{3.11}$$

giving $L_X=(0.03_{-0.006}{}^{+0.014})\,\mu$ at room temperature.

IV. HOT-ELECTRON SCATTERING MODEL FOR HIGHER PHOTON ENERGIES

For photon energies above 2.3 eV, the number of electrons emitted which are not thermalized becomes significant. The diffusion model is no longer sufficient to explain the experimental results, and we must consider in more detail the scattering process by which

[5] Frank Herman (private communication).

thermalization in the X minima occurs. The major scattering mechanism for hot electrons in the X minima is equivalent intervalley scattering by optical phonons for which the relaxation time is given by Conwell and Vassel[6]:

$$\frac{1}{\tau_{XX'}}=\frac{2}{3}\frac{D_{XX'}{}^2(m_X{}^{(N)})^{3/2}}{2^{1/2}\pi\hbar^3\rho\omega_{\rm opt}(e^\beta-1)}$$
$$\times[(E+\hbar\omega_{\rm opt}-E_X)^{1/2}+e^\beta(E-\hbar\omega_{\rm opt}-E_X)^{1/2}], \quad (4.1)$$

where E_X is the energy of the X minima, and $\hbar\omega_{\rm opt}$ is the optical phonon energy. For $E-E_X\gg\hbar\omega_{\rm opt}$,

$$1/\tau_{XX'}\approx C(E-E_X)^{1/2}, \quad (4.2)$$

where C is a temperature-dependent constant. For this energy dependence of τ, the mean free path is constant and will be defined as the scattering length l_s.

At each scattering event, the electron will lose or gain an energy equal to the optical phonon energy $\hbar\omega_{\rm opt}$. The average number of phonons with an energy $\hbar\omega_{\rm opt}$ at a temperature T is given from the Bose-Einstein distribution as

$$n_a=1/(e^\beta-1), \quad (4.3)$$

where $\beta=\hbar\omega_{\rm opt}/kT$.

The probability of an electron absorbing an optical phonon is proportional to n_a, while the probability of emitting a photon is proportional to n_a+1. Thus, the probability of gaining energy during a scattering event is given by

$$P_G=n_a/(2n_a+1)=1/(1+e^\beta). \quad (4.4)$$

The probability of losing energy during a scattering event is then

$$P_L=1-P_G. \quad (4.5)$$

As discussed earlier, we may calculate the exact excited energy distribution from the band structure throughout the Brillouin zone and the optical-transition matrix elements. Let this excited distribution function be given by $f_0(E)$, where $f_0(E)$ is normalized such that $\int_0^\infty f_0(E)dE=1$.

The distribution after one scattering event is then given by

$$f_1(E)=P_Gf_0(E-\hbar\omega_{\rm opt})+P_Lf_0(E+\hbar\omega_{\rm opt}). \quad (4.6)$$

Continuing this process, the distribution after n scattering events is given by

$$f_n(E)=P_Gf_{n-1}(E-\hbar\omega_{\rm opt})+P_Lf_{n-1}(E+\hbar\omega_{\rm opt})$$
$$=\sum_{l=0}^{n}\frac{n!}{l!(n-l)!}P_G{}^l(1-P_G)^{n-l}$$
$$\times f_0[E+(n-2l)\hbar\omega_{\rm opt}]. \quad (4.7)$$

The emitted energy distribution which can be externally observed is given by

$$f_{\rm emt}(E)=\sum_{n=0}^{\infty}P_nf_n(E), \quad (4.8)$$

where P_n is the probability that an electron will escape after n scatterings. P_n is a function of α and l_s. For the case of a constant scattering length l_s, this function has been calculated by Duckett[7] and is given in our notation by

$$P_n=\frac{1}{\pi(n+1)}\left\{\int_0^\infty\left[1-\left(\frac{\tan^{-1}\alpha l_sz}{\alpha l_sz}\right)^{n+1}\right]\frac{dz}{1+z^2}\right.$$
$$\left.-\sum_{j=1}^{n}P_{n-j}\int_0^\infty\left[1-\left(\frac{\tan^{-1}\alpha l_sz}{\alpha l_sz}\right)^{j}\right]\frac{dz}{1+z^2}\right\}. \quad (4.9)$$

In doing this scattering calculation for GaAs, we must take into account thermalization in the X minima. We may do this in a simple manner by assuming that above 1.75 eV, $f_{\rm emt}(E)$ is given as before by Eq. (4.8). Those electrons which would have scattered below 1.75 eV are assumed instead to remain at the energy of the X minima, giving

$$F_{\rm emt}(E)=f_{\rm emt}, \qquad \text{for } E>1.75$$
$$=\delta(E-1.75)\int_{-\infty}^{1.75}f_{\rm emt}(E)dE,$$
$$\text{for } E=1.75 \quad (4.10)$$
$$=0, \qquad \text{for } E<1.75.$$

In order to facilitate comparison with experiment, $F_{\rm emt}(E)$ is convolved with the normalized measured resolution function R of the experimental curves (see Sec. IX), giving for the observed distribution

$$f_{\rm obs}(E)=\int_{-\infty}^{\infty}F_{\rm emt}(E-\mu)R(\mu)d\mu. \quad (4.11)$$

In a practical calculation of $f_{\rm obs}$, we must terminate the summation of P_nf_n at some finite value of n. P_n drops off slowly for large n, so we must look at f_n. Because of the initial normalization of f_0,

$$\int_{-\infty}^{\infty}f_n(E)dE=1 \quad (4.12)$$

for all n. Scattering down in energy is more likely than scattering up in energy; therefore,

$$\int_{1.75}^{\infty}f_n(E)dE<\int_{1.75}^{\infty}f_{n-1}(E)dE. \quad (4.13)$$

[6] E. M. Conwell and M. O. Vassell, Phys. Rev. **166**, 797 (1968).

[7] Steven W. Duckett, Phys. Rev. **166**, 302 (1968).

We use the criterion

$$\int_{1.75}^{\infty} f_n(E)dE<0.05 \tag{4.14}$$

to terminate our calculation. This calculation has been done on a computer for a photon energy of 3.0 eV, using as a variable parameter the scattering length l_s. Figure 9 shows the comparison between this calculated distribution and the experimentally measured distribution. The computer solution for longer scattering lengths gives a larger high-energy peak, and that for shorter scattering lengths a smaller peak. Thus, by matching theoretical and experimental results, we are able to determine the hot-electron mean free path, $l_s=35\pm10$ Å, at room temperature.

Using this scattering length, we may determine the thermalization length L_T discussed earlier in conjunction with the assumption of rapid thermalization and transport by diffusion. The average energy lost in a scattering event is given by

$$\Delta E_s=(P_L-P_G)\hbar\omega_{\text{opt}}. \tag{4.15}$$

Thus, the average number of scattering events required for thermalization is

$$N=(E-E_x)/\Delta E_s. \tag{4.16}$$

Using a 3-dimensional random-walk model and identifying L_T with the standard deviation of the probability density function after N scatterings, we obtain

$$L_T=\tfrac{1}{2}(\sqrt{N})l_s. \tag{4.17}$$

For an electron initially excited to an energy of 2.0 eV, the thermalization length is $L_T=0.0076\,\mu$. This value of L_T easily satisfies $L_T\ll1/\alpha$ over the range of interest and gives $L_X\approx4L_T$, satisfying the requirement that $L_T\ll L_X$ as long as only modest accuracy is desired.

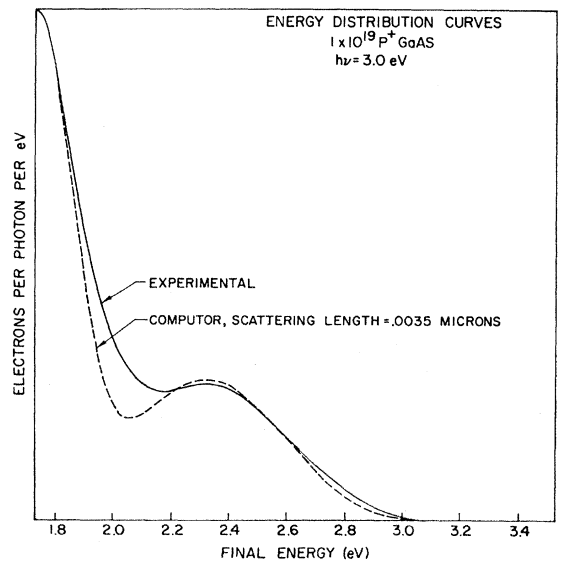

FIG. 9. Comparison of calculated and measured energy-distribution curves for an excitation at $h\nu=3.0$ eV. Electrons thermalized in the Γ_1 minima are not included in this figure.

V. CALCULATION OF INTERVALLEY COUPLING CONSTANTS

Using the value of l_s obtained, we may calculate the coupling constant for equivalent intervalley scattering. From Eq. (4.1) we have

$$\frac{1}{\tau_{XX'}}\approx\frac{2}{3}\frac{D_{XX'}{}^2(m_X{}^{(n)})^{3/2}(e^\beta+1)}{2^{1/2}\pi\hbar^2\rho(\hbar\omega_{\text{opt}})(e^\beta-1)}(E-E_X)^{1/2},$$

$$\text{for } E-E_X\gg\hbar\omega_{\text{opt}} \tag{5.1}$$

where everything except $D_{XX'}$ and $\tau_{XX'}$ are known. For a constant scattering length we have

$$1/\tau_{XX'}=v/l_s=(2^{1/2}/m^{*\frac{1}{2}}l_s)(E-E_X)^{1/2}. \tag{5.2}$$

Combining these equations and solving for $D_{XX'}$, we have

$$D_{XX'}=\left(\frac{e^\beta-1}{e^\beta+1}\frac{3\pi\hbar^2\rho(\hbar\omega_{\text{opt}})}{(m_X{}^{(n)})^{3/2}m^{*\frac{1}{2}}l_s}\right)^{1/2}. \tag{5.3}$$

Substituting our measured value of $l_s=35$ Å at room temperature gives

$$D_{XX'}=(1.5\pm0.2)\times10^9\text{ eV/cm}.$$

This value is probably somewhat high, because at the electron energies involved in the determination of l_s intervalley scattering to the L_1 and X_3 valleys and polar mode intravalley scattering are also possible. If we assume that the matrix elements for scattering to states in L_1 and X_3 are equal to that for scattering to equivalent X_1 valley states, and that the combined density of states for L_1 and X_3 is 30% of the density of states in the X_1 valleys,[8] we have as a better estimation

$$D_{XX'}=(1.3\pm0.2)\times10^9\text{ eV/cm}. \tag{5.4}$$

Using Eq. (4.1) we may calculate the mobility for equivalent intervalley scattering in X at 300°K,

$$\mu_{\text{eis}}=\frac{q}{m^*}\Bigg[3\pi\hbar^2\rho\omega_{\text{opt}}(e^\beta-1)\times\left\langle\frac{E-E_X}{(E-E_X+\hbar\omega_{\text{opt}})^{1/2}+e^\beta(E-E_X-\hbar\omega_{\text{opt}})^{1/2}}\right\rangle\Big/2^{1/2}D_{XX'}{}^2(m_X{}^{(n)})^{3/2}\langle E-E_X\rangle\Bigg] \tag{5.5}$$

$$=175\text{ cm}^2/\text{V sec}.$$

[8] Estimated from a plot of equal energy contours in the (110) plane and symmetry considerations. It is the ratio of the density of states available for scattering into at a fixed electron energy, and not the ratio of the density of states referred separately to each minima.

Combining this with Conwell and Vassel's[6] value for polar mode intervalley scattering, and with Harris's recently measured values for deformation potential scattering,[9] we obtain

$$\mu_X = 120 \text{ cm}^2/\text{V sec}. \tag{5.6}$$

This compares with experimental values of 155 $\text{cm}^2/\text{V sec}$ [10] and 110 $\text{cm}^2/\text{V sec}$ [11] for GaAs, and a value of 110 $\text{cm}^2/\text{V sec}$ for GaP.[12]

Using the Einstein relationship to determine the diffusion constant gives

$$D_X = (kT/q)\mu_X = 3.1 \text{ cm}^2/\text{sec}. \tag{5.7}$$

Using this value of diffusion coefficient and the measured value of $L_X = 0.03\ \mu$, we obtain the scattering time for scattering from X to Γ,

$$\tau_{X\Gamma} = L_X^2/D_X = (2.9_{-1.1}^{+3.3}) \times 10^{-12} \text{ sec}. \tag{5.8}$$

From Conwell and Vassell[6] we have

$$\frac{1}{\tau_{X\Gamma}} = \frac{D_{\Gamma X}^2 m_1^{3/2}}{2^{1/2}\pi\hbar^3\rho\omega_{\text{opt}}} \frac{1}{e^\beta - 1}[\gamma^{1/2}(E - E_\Gamma + \hbar\omega_{\text{opt}}) \times \gamma'(E - E_\Gamma + \hbar\omega_{\text{opt}}) + e^\beta \gamma^{1/2}(E - E_\Gamma - \hbar\omega_{\text{opt}}) \times \gamma'(E - E_\Gamma - \hbar\omega_{\text{opt}})]. \tag{5.9}$$

For a distribution thermalized in the X minima, $(E - E_X \ll \hbar\omega_{\text{opt}}) \ll E_X - E_\Gamma$, giving

$$\frac{1}{\langle\tau_{X\Gamma}\rangle} \approx \frac{D_{\Gamma X}^2 m_1^{3/2}}{2^{1/2}\pi\hbar^2\rho(\hbar\omega_{\text{opt}})} \frac{e^\beta + 1}{e^\beta - 1} \times [\gamma^{1/2}(E_X - E_\Gamma)\gamma'(E_X - E_\Gamma)]. \tag{5.10}$$

We may solve this equation for $D_{\Gamma X}$, giving

$$D_{\Gamma X} = (3.8_{-1.2}^{+0.9}) \times 10^8 \text{ eV/cm}. \tag{5.11}$$

For this value of $D_{\Gamma X}$, the energy dependence of the Γ to X scattering time at room temperature is shown in Fig. 10, along with the scattering time for polar optical and acoustic scattering, as calculated by Conwell and Vassel.[6] For an electron excited to an energy higher than 0.016 eV above the X_1 minima, the most likely scattering event is a scattering from the Γ_1 to the X_1 minima. Thus, the assumption used in the calculation of F_Γ and F_X, that all electrons excited to energies higher than 1.75 eV could be considered to scatter almost instantly into an X_1 minima, is well justified.

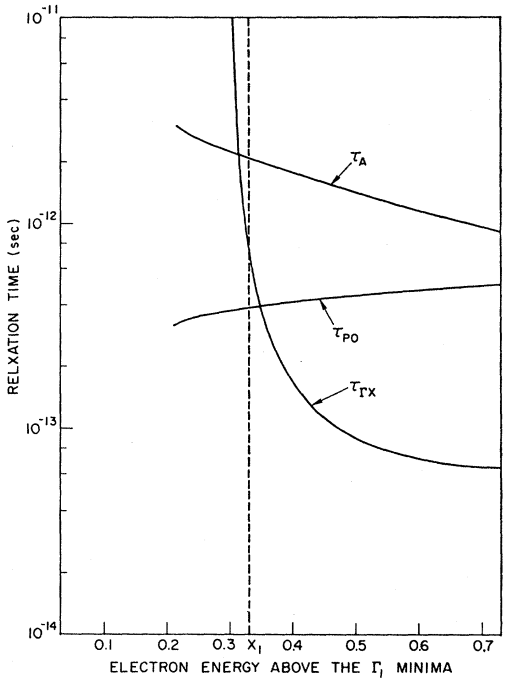

FIG. 10. Scattering times for Γ_1 to X_1 scattering, polar optical scattering, and acoustic scattering for hot electrons in the Γ_1 minima.

VI. TEMPERATURE DEPENDENCE OF THE X MOBILITY AND DIFFUSION LENGTH

At liquid-nitrogen temperatures, impurity scattering and acoustic phonon scattering are more important than equivalent intervalley scattering in determining the mobility in the X minima. In order to obtain an accurate temperature dependence of the X mobility and diffusion length, we must include several types of scattering. These are plotted in Fig. 11.

The mobility for equivalent intervalley scattering is given by Eq. (5.5), where the indicated averages were obtained by numerical integration.

For intravalley acoustic scattering, using Harris's recently measured values[9] of $\Xi_d = 16.8$ eV and $\Xi_\mu = -4.6$ eV, we obtain

$$\mu_A = \frac{4\pi\hbar^4 c_l q}{9(2\pi)^{1/2}(m_X^* k_0 T)^{3/2}}\left(\frac{1}{m_l \Xi_l^2} + \frac{2}{m_t \Xi_t^2}\right) = 2.9 \times 10^6/T^{3/2} \text{ cm}^2/\text{V sec}. \tag{6.1}$$

From Eq. (5.10), $\tau_{X\Gamma}$ is given by

$$\tau_{X\Gamma} = 5.4 \times 10^{-12}[(e^\beta - 1)/(e^\beta + 1)] \text{ sec}, \tag{6.2}$$

which is plotted in Fig. 12. The mobility for scattering to Γ_1 is given by

$$\mu_{X\Gamma} = q\tau_{X\Gamma}/m_X^*. \tag{6.3}$$

From Conwell and Vassel,[6] the mobility for polar optical scattering at room temperature is approximately

[9] J. S. Harris, Ph. D. thesis, Stanford University, 1968 (unpublished).
[10] G. King, J. Lees, and M. P. Wasse, quoted by P. N. Butcher and W. Fawcett, Phys. Letters **21**, 489 (1966).
[11] A. R. Hutson, A. Jayaraman, and A. S. Coriell, Phys. Rev. **155**, 786 (1967).
[12] D. N. Nasledor and S. V. Slobalchikor, Fiz. Tverd. Tela **4**, 2755 (1962) [English transl.: Soviet Phys.—Solid State **4**, 2021 (1963)].

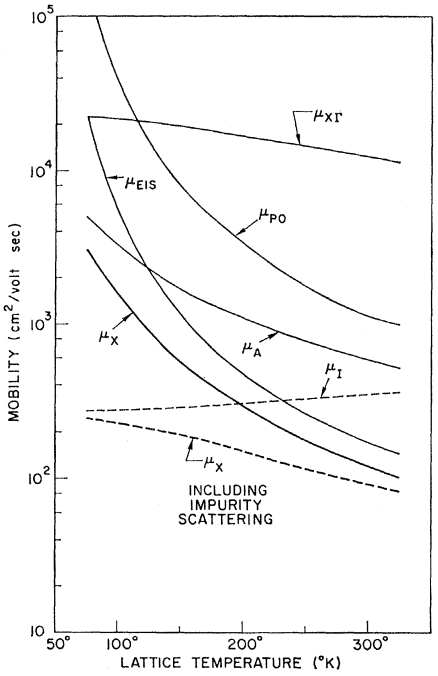

FIG. 11. Temperature dependence of the various mechanisms which determine the mobility in the X_1 minima. Solid lines are for a lightly doped sample. Dashed lines include impurity scattering.

$6\mu_{eis}$. The temperature dependence should be the same as for equivalent intervalley scattering, so we assume

$$\mu_{po} \approx 6\mu_{eis}. \tag{6.4}$$

In any case, μ_{po} is sufficiently larger than both μ_{eis} and μ_A over the entire temperature range so that the value of mobility in the X minima is insensitive to the exact value of μ_{po}.

The mobility in the X minima for an impurity-free sample, shown as the heavy line in Fig. 11, is given by

$$\mu_X = q\langle\tau_X\rangle/m^* \tag{6.5}$$

$$\approx (1/\mu_{eis}+1/\mu_A+1/\mu_{X\Gamma}+1/\mu_{po})^{-1}. \tag{6.6}$$

At the high doping levels involved in this experiment, impurity scattering must also be considered. To our knowledge, no really good theory exists for minority carrier scattering time at high doping concentrations for ionized impurity scattering or electron-hole scattering. Undoubtedly the holes screen the ionized acceptors to some extent. We have approximated these types of scattering with the Mansfield impurity scattering model,[13] modified to use the hole density of states effective mass to calculate the screening potential, and an electron effective mass of $0.25m_0$ to calculate the resultant mobility, giving the dashed curve shown in Fig. 11 as μ_I. At the 3×10^{19}/cm³ doping level of this sample, it is necessary to include the effects of degeneracy. The Mansfield formula is therefore used to calculate the screening length, and Boltzmann statistics are used for the electrons in the conduction band.

The X mobility including impurity scattering is also shown in Fig. 11. From Eq. (6.5), $\langle\tau_X\rangle = 2.1\times10^{-14}$ sec at 300°K and 5.8×10^{-14} sec at 77°K. Thus,

$$\tau_{X\Gamma} \gg \langle\tau_X\rangle \tag{6.7}$$

in both cases, and the concept of a thermalized distribution diffusing in the X minima is valid throughout the temperature range. The diffusion length is given by

$$L_X = [(kT/q)\mu_X\tau_{X\Gamma}]^{1/2}, \tag{6.8}$$

and is plotted in Fig. 13, along with three experimental points. The point at 130°K was the maximum experimental diffusion length. These experimental points were obtained by measuring the yield from the X minima versus temperature using Eq. (3.7), where F_X and α are obtained by shifting the 300°K values to a higher energy corresponding to the shift in the band gap. P_X increases slightly as the temperature is lowered.

The experimental and theoretical diffusion lengths are in qualitative agreement in that both increase as the temperature is decreased. The experimental increase is, however, significantly more than the theoretical increase. We believe that the physical reasons for this disagreement relate to the finite number of scatterings before the energy drops to the optical phonon energy, and a finite rate of finally settling down to a Boltzmann distribution characterized by the lattice temperature. Both of these effects result in an overestimation of the impurity scattering cross section in the mobility theory.

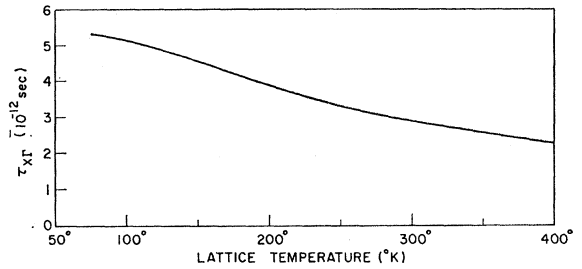

FIG. 12. Temperature dependence of the X_1 to Γ_1 scattering time.

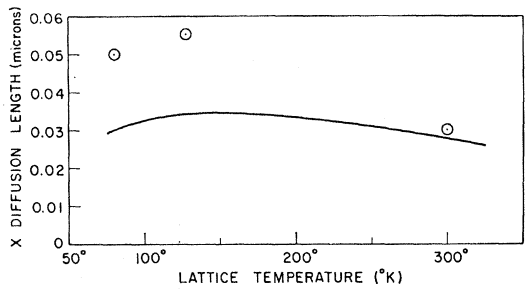

FIG. 13. Experimental (points) and theoretical (line) temperature dependence of the X diffusion length.

[13] R. Mansfield, Proc. Phys. Soc. (London) **B69**, 76 (1956).

An arbitrary increase of the relatively temperature-independent impurity mobility by a factor of approximately 3 gives an adjusted theory that is in line with experiment.

VII. TEMPERATURE DEPENDENCE OF THE HOT-ELECTRON SCATTERING LENGTH

From Eqs. (5.1) and (5.2) we see that

$$l_s = K[(e^\beta - 1)/(e^\beta + 1)], \tag{7.1}$$

where K is a temperature-independent constant. Thus, we have

$$l_s(80°\text{K}) = 1.8 l_s(300°\text{K}) = 63\ \text{Å}. \tag{7.2}$$

On the other hand, from Eqs. (4.4), (4.5), and (4.15) we see that the average energy lost per scattering event is also proportional to $(e^\beta - 1)/(e^\beta + 1)$, giving

$$\Delta E_s(80°\text{K}) = 1.8 \Delta E_s(300°\text{K}). \tag{7.3}$$

Thus, we have two counteracting effects and might expect only a small change with temperature in the high-energy part of the emitted distribution. Both the computer model (assuming no change in α with temperature, but with $l_s = 63$ Å) and the experimental data (shown in Fig. 14) show a small increase in the number of high-energy electrons at liquid-nitrogen temperature.

VIII. TEMPERATURE DEPENDENCE OF THE LOCATION OF THE CONDUCTION BAND MINIMA

Since we can see electrons thermalized in the conduction band minima in a photoemission experiment, our data offers a very direct method of measuring the energy of these minima.

In the measurement of an electron energy-distribution curve (EDC), the energy scale is derived from the retarding potential applied between the emitter and the collector can. Errors in the measurement of spacing between two pieces of structure can be introduced by stray fields which are present in the experimental apparatus.

An extraneous field component parallel to the retarding field will cause a uniform shift in the energy scale of the EDC, introducing no errors in the measurement of structure spacing, except for electrons with almost zero kinetic energy. For the case of almost zero kinetic energy, there can be an apparent shift to a lower measured energy if the parallel field component changes direction along the electron trajectory. This shift will increase the measured structure spacing.

TABLE II. Numerical values used in calculations.

$C_l = \rho \mu_l^2$
$\hbar\omega_{\text{opt}} = 0.03$ eV
$m_X^{(n)} = 1.2 m_0$
$m^* = 0.41 m_0$
$m_l = 0.065 m_0$
$\rho = 5.31$ g/cm^3
$q = 1.602 \times 10^{-19}$ C
$\mu_l = 5.22 \times 10^5$ cm/sec

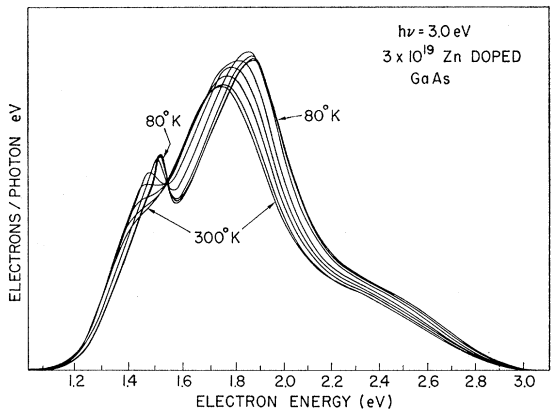

FIG. 14. Energy-distribution curves for a 3×10^{19}/cm^3 Zn-doped sample for a photon energy of 3.0 eV over a temperature range of 80–300°K.

An extraneous field component perpendicular to the retarding field will give a resultant field

$$F_T = (F_{APP}^2 + F_\perp^2)^{1/2}, \tag{8.1}$$

where F_T is the total field seen by the electron, F_{APP} is the desired retarding field, and $E_\perp$ is the extraneous perpendicular field. Looking at the change in total field with respect to a change in applied field, we see that

$$dF_T/dF_{APP} = F_{APP}/(F_{APP}^2 + F_\perp^2)^{1/2} \leq 1. \tag{8.2}$$

This means that the change in field seen by the electron at every point along its trajectory is less than or equal to the change in applied field, thus the spacing in energy between two pieces of structure as measured on an experimental energy-distribution curve will be greater than or equal to the actual spacing in energy.

If there is a rapidly varying threshold escape function $[C_E(E)]$ near one peak (the lower peak), the apparent peak in the emitted electron distribution is at the point where

$$\frac{d}{dE}[f(E)C_E(E)] = f(E)\frac{dC_E(E)}{dE} + C_E(E)\frac{df(E)}{dE} = 0. \tag{8.3}$$

Since $C_E(E)$ is a monotonically increasing function of E, $dC_E(E)/dE > 0$, giving $df(E)/dE < 0$ at the measured peak. Thus, the apparent peak is on the high-energy side of the actual peak.

If $f(E)$ is assumed to be a Guassian distribution of the form

$$f(E) \propto e^{-[(E-E_0)/\Delta E]^2}, \tag{8.4}$$

then the apparent shift in the peak position is given by

$$\delta_E = [(\Delta E)^2/2C_E](dC_E/dE). \tag{8.5}$$

For our room-temperature experimental data, $\Delta E \approx 0.1$ eV. The energy dependence of C_E is not known exactly, but from the data in Sec. IX, we estimate $C_E(1.4 \text{ eV}) = 0.1$ and $(dC_E/dE)(1.4 \text{ eV}) < 0.2$ for a Cs+(O+Cs)[2] surface treatment, giving $\delta_E < 0.01$ eV.

At liquid-nitrogen temperature ΔE becomes much smaller, and δ_E is completely negligible.

From Eq. (8.2), it is clear that the largest errors will occur for small applied fields, that is for low energy (Γ_1) electrons. In our experimental apparatus, every attempt has been made to reduce stray fields to the smallest possible values. The measured separation between the Γ_1 and X_1 peaks at room temperature in our best experimental data is 0.35 eV. In this case, the effect of the threshold function is negligible (of the order of 0.01 eV). The actual separation is almost certainly less than 0.35 eV. We can estimate the error still present in this measurement by using the second derivative method[14] for locating the final energy states of the vertical transitions, and measuring back from the energy of these states (assumed to be at $E = h\nu$ because of the large ratio of effective masses) to the location of the X_1 peak. Using Sturge's[15] value for the band gap of 1.425 eV at 300°K, this measurement shows that the spacing between the Γ_1 and X_1 minima can be no less than 0.28 eV. Our best estimate of the actual separation is 0.33 eV.

Because of the smaller energy differences involved, the change in the position of a conduction band minima with temperature may be determined more accurately than its relative position with respect to other minima.

Figure 14 shows a similar series for a photon energy of 3.0 eV. Figure 15 shows a series of energy distribution curves for a photon energy of 1.6 eV taken over a range of temperatures between 80 and 300°K. Both sets of curves are for a $3\times10^{19}/\text{cm}^3$ Zn-doped sample. In cooling from 300–80°K, the Fermi level moves down 0.01 eV. Subtracting this value from the measured energy shifts, we see that the band gap increases 0.09 ± 0.02 eV, and the energy of the X_1 minima increases 0.11 ± 0.02 eV, when the temperature is reduced from 300 to 80°K. The shift of 0.09 eV in the band gap agrees with Sturge's[15] measurement of the band gap shift, giving us confidence that δ_E from Eq. (8.5) is in fact small enough to be neglected over the entire temperature range. Our best estimate of the Γ_1 to X_1 spacing at liquid-nitrogen temperature is 0.35 eV, which agrees well with the value of 0.36 eV obtained by extrapolating high-temperature Hall data to 0°K.[16] However, our data are in conflict with the recently claimed value of 0.44 eV [17] and the commonly used value of 0.36 eV at room temperature. A decrease in Γ_1 to X_1 spacing with an increase in temperature is consistent with the temperature dependence of the Gunn-effect threshold field.[18]

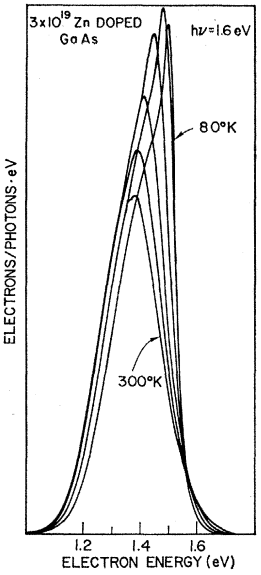

FIG. 15. Energy-distribution curves for a $3\times10^{19}/\text{cm}^3$ Zn-doped sample for a photon energy of 1.6 eV over a temperature range of 80–300°K.

Figure 16 shows the location of the conduction band minima versus lattice temperature, assuming a quadratic temperature dependence between experimental points which are shown with bars indicating the possible error range. The zero of the energy scale is defined from Sturge's value of the band gap[15] at 300°K.

At 80°K, two pieces of structure are visible below the Γ_1 minimum. Their exact location is determined from the derivative of the energy-distribution curve.

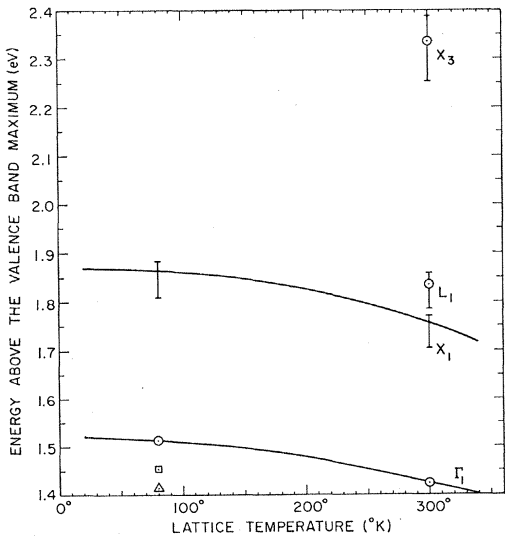

FIG. 16. Temperature dependence of the location of conduction band minima indicating best estimates and possible error ranges. The error range for the location of the L_1 and X_3 minima comes principally from the possible error in the location of the X_1 minima, X_1 to L_1 spacing is known more accurately (Ref. 14).

[14] L. W. James, R. C. Eden, J. L. Moll, and W. E. Spicer, Phys. Rev. **174**, 909 (1968).
[15] M. D. Sturge, Phys. Rev. **127**, 768 (1962).
[16] H. Ehrenreich, Phys. Rev. **120**, 1951 (1960).
[17] Ivan Balslev, Phys. Rev. **173**, 762 (1968).
[18] John Copeland (private communication).

If the sample is illuminated with a phonon energy of 1.46 eV, the structure at 1.455 eV, indicated by the square in Fig. 16, is no longer present in the energy-distribution curve, and the structure at 1.415 eV is a dominant peak. Thus, the structure at 1.415 eV corresponds to a definite state (the origin of which is as yet unknown) to which photoexcitation can occur.

The structure at 1.455 eV corresponds to a state to which direct photoexcitation is impossible; it is present only when electrons in the Γ_1 minimum are present. Its location at 0.06 eV below the Γ_1 minima prohibits identifying it with electrons which have undergone an optical phonon scattering event in the band-bending region; the optical phonon energy is 0.03 eV. There is no reason to believe that electrons which have undergone two scattering events should produce a definite structure in the energy-distribution curve, when those scattering only once do not.

When an electron is accelerated through the band-bending region and strikes the potential barrier at the surface, it has some chance of being reflected rather than being emitted. We believe that the peak at 1.455 eV is electrons which have been reflected once and are then emitted.

IX. DETAILS OF THE ESCAPE PROCESS

The sharp peak visible in the liquid-nitrogen energy-distribution curves indicates that the experimental apparatus is capable of extremely high resolution, and that the measured widths of the Γ_1 and X_1 peaks are in fact their actual widths. Here we will look in detail at the physical processes which are responsible for the width of these peaks, and show how they relate to the details of the escape process which determine escape probability.

For electrons thermalized in a parabolic conduction band minima, the distribution in initial-state energies is proportional to $E^{1/2}e^{-E/kT}$. The width at half-amplitude of this distribution in the bulk of the crystal before entering the band-bending region is given by

$$\Delta E_T \approx 1.5kT = 0.04 \text{ eV} \tag{9.1}$$

at room temperature.

The field in the band-bending region is approximately

$$F = \Delta E \text{ (band bending)}/W = 720\,000 \text{ V/cm}, \tag{9.2}$$

considerably beyond the point where saturated drift velocity is reached; thus, most electrons will be heated in the Γ_1 minima and will be transferred into the X_1 minima at the first scattering event. For $D_{\Gamma X}=3.8\times10^8$, the time to scatter into X_1 is approximately equal to $\langle\tau_X\rangle$ at room temperature. (The exact time is energy-dependent and shown in Fig. 10.) The probability that an electron will undergo n scattering events while passing through the band-bending region is given approximately by the Poisson distribution

$$P_n = \frac{e^{-W/l_s}(W/l_s)^n}{n!}. \tag{9.3}$$

From Eqs. (4.7) and (4.8), the emitted energy distribution for an initially thermalized distribution in a conduction band minima at E_0 is given by

$$f_{\text{emt}}(E) = \sum_{n=0}^{\infty} e^{-W/l_s}\left(\frac{W}{l_s}\right)^n \sum_{l=0}^{n} \frac{P_G{}^l(1-P_G)^{n-l}}{l!(n-l)!} \times[E-E_0+(n-2l)\hbar\omega_{\text{opt}}]^{1/2} \times\exp\left(-\frac{[E-E_0+(n-2l)\hbar\omega_{\text{opt}}]}{kT}\right) \times u[E-E_0+(n-2l)\hbar\omega_{\text{opt}}], \tag{9.4}$$

where

$$u(x)=1, \quad \text{for } x\geq 0$$
$$=0, \quad \text{for } x<0.$$

For the parameters valid for GaAs with a doping of $3\times10^{19}/\text{cm}^3$ at room temperature, this calculation yields an approximately Guassian distribution with a width at half-amplitude of 0.09 eV and a peak at approximately 0.01 eV below the energy of the Γ minimum.[19]

For an electron 0.2 eV above the bottom of the X_1 minima (valid for an electron near the surface in the band-bending region which was originally thermalized in the Γ_1 minimum), the time between scattering events is given by Eq. (5.2). $\tau_{XX'}=1.32\times10^{-14}$ sec at room temperature. The accuracy with which the electron energy may be defined is limited by the uncertainty principle. The width at the half-amplitude points of a measured energy distribution (assuming a Lorenzian line shape from a single energy level) is given for $\tau_{XX'}=1.32\times10^{-14}$ sec by

$$\Delta E_\tau = \hbar/\tau_{XX'} = 0.08 \text{ eV}. \tag{9.5}$$

Combining this lifetime broadening effect with the width of the emitted distribution calculated above, we obtain an expected half-amplitude width of 0.12 eV for the observed energy distribution of electrons thermalized in the Γ_1 minima at room temperature. The actual experimental curves show a half-width of 0.20 eV. The reason for the additional width is made clear by examining the liquid-nitrogen data.

At liquid-nitrogen temperature, we have a different situation. The half-amplitude width of the initial thermalized distribution is 0.01 eV. From Eq. (9.3),

[19] This peak position may be understood from the following argument. The peak in the initial electron distribution is at $kT/2=0.013$ eV above the Γ minima. The average electron suffers $n=W/l_s=1.43$ collisions. The average energy lost in a scattering event is $(P_L-P_G)\hbar\omega_{\text{opt}}=0.016$ eV. Thus, 0.023-eV average energy is lost in 1.43 scattering events, giving a peak at (0.023−0.013) eV=0.01 eV below the Γ minima.

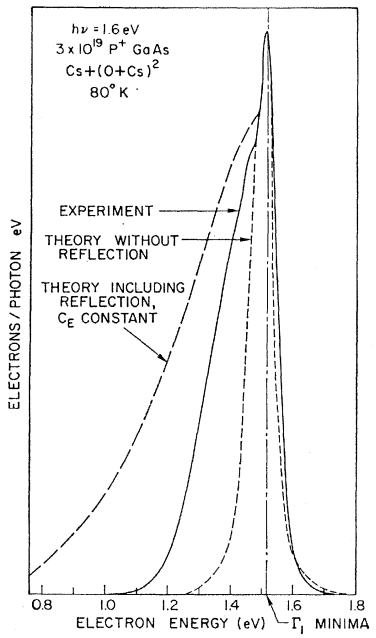

FIG. 17. Comparison between theory and experiment for the shape of the 80°K energy-distribution curve.

$P_0 > P_n$, where $n>0$; that is, more electrons will cross the band-bending region without scattering than will undergo any given number of scattering events while crossing. This, coupled with the fact that the probability for gaining energy during a scattering event is practically zero, leads to a skewed distribution with a peak at the Γ_1 energy point, and a tail going to lower energies. After combining this distribution with the lifetime broadening (0.043-eV half-amplitude width), we obtain the results shown as the short-dashed theoretical curve in Fig. 17. Comparison with the experimental curve shows good agreement in shape at the high-energy end of the curve and a large discrepancy in the low-energy tail. The theoretical curve, if drawn to scale, would be eight times as high as the experimental curve at the peak. The theory on the width of the energy-distribution curve to this point has assumed that all electrons which reach the surface are emitted. From the measured escape probabilities, we know that this is not the case. From the actual value of the peak height of the experimental and theoretical curves, we can estimate for this sample that roughly 12% of the electrons which strike the surface (with an energy of 1.5 eV above the valence band maximum in the bulk) are emitted the first time they strike the surface. We define this percentage which escapes upon hitting the surface once as the escape coefficient C_E.

A certain fraction of the electrons which strike the surface will be trapped in surface states and recombine. This fraction will be given by the surface trapping coefficient C_{ST}. We note that C_{ST} is determined by the quality of the material and the method of surface preparation, cleaved surfaces giving the lowest value observed so far. Some boat-grown material has been found to have a moderately high value of C_{ST} even for cleaved surfaces.

Those electrons which are not emitted or trapped will be reflected back into the band-bending region, giving a reflection coefficient $C_R = 1 - C_E - C_{ST}$. The structure in the liquid-nitrogen energy-distribution curves 0.06 eV below the Γ_1 minima is identified with once-reflected electrons; thus, the electrons are assumed to lose 0.06 eV at each reflection. After being reflected, the electrons are reaccelerated toward the surface (some of them undergoing optical phonon scattering in the process) and strike the surface again.

For hot electrons where C_E and C_{ST} change slowly with electron energy, and where an electron may undergo many reflections before losing enough energy that it drops below the vacuum level, the escape probability is given by

$$P = C_E/(C_{ST}+C_E). \tag{9.6}$$

For X_1 and Γ_1 electrons, dropping below the vacuum level cannot be ignored. The simplest estimate of escape probability for this case ignores optical phonon scattering in the band-bending region and assumes a sharp cutoff of C_E at the vacuum level, giving

$$P = C_E \sum_{n=0}^{l} C_R{}^n, \tag{9.7}$$

where l is the next integer smaller than

$$(E_{\min} - E_{\text{vac level}})/0.06,$$

and C_E/C_R is assumed constant as C_{ST} varies. This calculation is shown in Fig. 18 for the case of an optimum [Cs+(O+Cs)⁶] surface treatment.[20] (Absorption in the (O+Cs) layers neglected.) This is intended as a

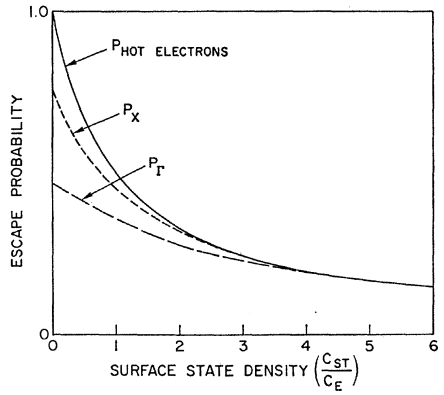

FIG. 18. Estimate from a simplified model of the effect of surface states on escape probability.

[20] L. W. James, J. L. Moll, and W. E. Spicer, Proceedings of the 1968 International Conference on GaAs, Dallas, Texas (unpublished).

rough estimate of escape probability variation with surface state density and not as an exact calculation. C_E/C_R is undoubtedly a function of electron energy.

For the sample of Fig. 17, the maximum escape probability measured is 0.4, giving, from Eq. (9.6), $C_{ST}=0.18$ and $C_R=0.70$. Using these values and introducing reflection into the model, we obtain the long-dashed theoretical curve shown in Fig. 17. The theorectical curve is now drawn with the proper magnitude scale. The remaining difference between the theoretical and experimental curves is due to the fact that C_E and C_{ST} are functions of the electron energy rather than constants. Not enough data is available to determine these functions quantitatively. C_E is zero for energies below the vacuum level, and increases with increasing electron energy. The energy of the bottom of the tail of the measured EDC is therefore a good measurement of the energy of the vacuum level.[20]

Comparison of the energy-distribution curves for low-yield (C_{ST} high) and high-yield (C_{ST} negligible) samples show that low-energy electrons are more adversely affected by high surface state densities than high-energy electrons, indicating that C_{ST} decreases with increasing electron energy, as expected.

By adding 30 (O+Cs) layers to the surface, we lower the vacuum level far enough[20] that C_E no longer varies rapidly with energy. Figure 19 shows the comparison between theory and experiment for this case. The theoretical curve has been multiplied by 0.25 to take into account absorption in the (O+Cs) layers. The agreement is now good.

In Fig. 17 the ratio between the area under the experimental curve and the area under the long-dashed theoretical curve, multiplied by the maximum escape probability (0.4), gives the Γ escape probability, which is 0.22 at liquid-nitrogen temperature for this sample and surface treatment.

The difference between the measured (0.20 eV) and calculated (0.12 eV) half-amplitude widths for the Γ_1 peak at room temperature can also be accounted for by multiple reflections at the surface.

Half-amplitude width of the peak corresponding to electrons in the X minima cannot be measured directly because of the presence of Γ electrons and hot electrons, but the X peak appears slightly wider than the Γ peak. This is expected for two reasons. First, there is no cutoff of the low end of the distribution by electrons scattering to an energy lower than the vacuum level. Second, τ in the band-bending region is smaller for

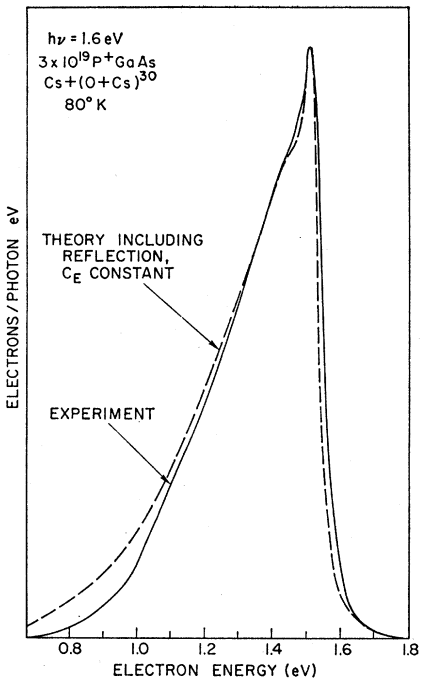

FIG. 19. Comparison between theory and experiment for the shape of the 80°K energy-distribution curve for the case of C_E constant.

electrons initially thermalized in X, both from the energy dependence of $\tau_{XX'}$ and from the fact that scattering to states in the X_3 minima is energetically possible as well as equivalent intervalley scattering. A smaller τ means a larger lifetime broadening of the distribution.

Examining Fig. 17 we can see that if the probability of escaping with no collisions were reduced by 20–30%, the sharp peak corresponding to unscattered electrons would be buried in the broader distribution. Apparently this is true for X electrons, the X distribution shows no such sharp structure.

ACKNOWLEDGMENTS

The authors would like to thank Professor W. E. Spicer, Dr. Frank Herman, A. P. Smith, J. S. Harris, and A. D. Baer for many useful discussions. They would also like to thank P. McKernan for his excellent technical support in the construction of the high-vacuum experimental apparatus.